

# The stability and work function of TaC<sub>x</sub>N<sub>1-x</sub> alloy surfaces

H. Zhu, and R. Ramprasad

Citation: *Journal of Applied Physics* **109**, 083719 (2011); doi: 10.1063/1.3580257

View online: <https://doi.org/10.1063/1.3580257>

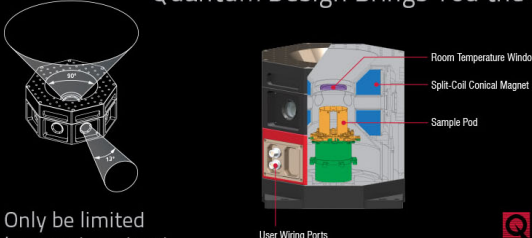
View Table of Contents: <http://aip.scitation.org/toc/jap/109/8>

Published by the *American Institute of Physics*

---

---

Quantum Design Brings You the Next Generation Magneto-Optic Cryostat




Only be limited by your imagination...

[Learn More](#)

Quantum Design  
qdusa.com/opticool5

8 Optical Access Ports: 7 Side; 1 Top  
Temperature Range: 1.7 K to 350 K  
7 T Split-Coil Conical Magnet  
Low Vibration: <10 nm peak-to-peak  
89 mm x 84 mm Sample Volume  
Automated Temperature & Magnet Control  
Cryogen Free



## The stability and work function of TaC<sub>x</sub>N<sub>1-x</sub> alloy surfaces

H. Zhu and R. Ramprasad<sup>a)</sup>

Department of Chemical, Materials and Biomolecular Engineering, Institute of Materials Science, University of Connecticut, 97 North Eagleville Road, Storrs, Connecticut 06269, USA

(Received 8 February 2011; accepted 12 March 2011; published online 25 April 2011)

The stability and work function of the (001), (110), and (111) surfaces of ordered TaC<sub>x</sub>N<sub>1-x</sub> crystals with various possible terminations were studied using density functional theory calculations. Among all surfaces considered, those with (001) orientations were found to be the most stable. The work function of these (001) stable surfaces increases monotonically from the pure TaN value of 3.3 eV to the pure TaC value of 3.8 eV. However, this variation is far surpassed by the strong dependence of the work function on the surface orientation and chemistry, regardless of the bulk alloy composition. © 2011 American Institute of Physics. [doi:10.1063/1.3580257]

### I. INTRODUCTION

Transition metal nitrides and carbides have found applications as diffusion barriers in semiconductor devices and refractory coatings for thermal protection because of their high thermal stability, dense interstitial structure, and low resistivity.<sup>1,2</sup> More recently, these systems have been considered and optimized as replacements for the poly-Si gate electrodes in next-generation transistors composed of high dielectric constant, or “high-*K*,” dielectrics.<sup>3</sup> In particular, TaC<sub>x</sub>N<sub>1-x</sub> and TiC<sub>x</sub>N<sub>1-x</sub> are attractive, as methods to deposit and process them are already well developed in the semiconductor industry. Moreover, these alloys have low vacuum work functions (WFs) that may be tuned by the alloy composition modulation,<sup>4,5</sup> an important requirement guiding the choice of the metal electrode.

Accordingly, many experimental and theoretical efforts have been devoted to transition metal carbides and nitrides. However, most of these studies have dealt with the bulk properties (i.e., the bulk modulus and phase stability)<sup>6</sup> and much less is known about the properties of their surfaces such as surface energies and WFs, barring a few studies of the ternary end-members TaC, TaN, TiC, and TiN.<sup>7-9</sup>

Following our recent work on the stability and WF of TiC<sub>x</sub>N<sub>1-x</sub> ternary alloy surfaces,<sup>10</sup> we have applied similar techniques to study TaC<sub>x</sub>N<sub>1-x</sub> alloy surfaces through *ab initio* density functional theory (DFT) based simulations. Among the possible phases for TaC<sub>x</sub>N<sub>1-x</sub> (the NaCl or CoSn structures),<sup>2,11,12</sup> the NaCl-type TaC<sub>x</sub>N<sub>1-x</sub> is the most desirable phase for the gate electrode application due to the low electrical resistivity. Thus, we focus on the NaCl-type TaC<sub>x</sub>N<sub>1-x</sub> solid solution in this paper. Our results reveal that the TaC<sub>x</sub>N<sub>1-x</sub> alloy behaves similar to TiC<sub>x</sub>N<sub>1-x</sub> in two ways: (1) the most stable surface is mainly (001) type; (2) the surface chemistry (i.e., orientation and defect density) plays the most important role in determining the WF. However, the impact of the defects on the WF of TaC<sub>x</sub>N<sub>1-x</sub> and TiC<sub>x</sub>N<sub>1-x</sub> is different. For example, carbon vacancies increase the WF of TaC<sub>x</sub>N<sub>1-x</sub> but decrease that of TiC<sub>x</sub>N<sub>1-x</sub>.

This paper is organized as follows. In Sec. II, we discuss the details of DFT calculations. Section III provides the bulk

properties of TaC<sub>x</sub>N<sub>1-x</sub> (such as the structure, stability, and density of states). In Sec. IV, we first address the methodology to compute the surface phase diagram for a ternary system and then discuss the surface stability of TaC<sub>x</sub>N<sub>1-x</sub> alloys. The WF for different bulk composition (or *x* value), surface orientation, and chemistry will be presented in Sec. V. Section VI summarizes our conclusions. A detailed comparison between TaC<sub>x</sub>N<sub>1-x</sub> and TiC<sub>x</sub>N<sub>1-x</sub> is given in each section.

### II. COMPUTATIONAL DETAILS

Our DFT calculations were performed using the Vienna *ab initio* simulation package<sup>13</sup> with the PW91 generalized gradient approximation,<sup>14</sup> Vanderbilt ultrasoft pseudopotentials,<sup>15</sup> and a cutoff energy of 315 eV for the plane wave expansion of the wave functions. The calculated results were converged with the atomic forces smaller than 0.04 eV/Å. The conventional cell of NaCl-type TaN is shown in Fig. 1(a) along with its primitive unit cell containing 1 Ta and 1 N atom (the white rhombohedron). To obtain homogeneous TaC<sub>x</sub>N<sub>1-x</sub> (*x* = 0, 0.25, 0.5, 0.75, and 1), we created a supercell of TaN with 2 × 2 × 2 primitive cells (containing 8 Ta and 8 N atoms) and then substituted the N atoms in the supercell by C in a systematic way as has been done earlier.<sup>10</sup> The supercell of bulk TaC<sub>x</sub>N<sub>1-x</sub> alloys for *x* = 0.25 thus contains 6 N and 2 C atoms and for *x* = 0.5 contains 4 N and 4 C atoms. As Fig. 1 shows, TaC<sub>0.75</sub>N<sub>0.25</sub> and TaC have similar configurations to TaC<sub>0.25</sub>N<sub>0.75</sub> and TaN, respectively, except that the identity of C and N are interchanged. These bulk calculations required a 5 × 5 × 5 *k*-point mesh for well-converged results.

Our surface calculations for five alloy compositions were performed using symmetric slab supercells containing 11 atomic layers and a 10 Å vacuum region. The (001), (110), and (111) surfaces involved 2 × 2, 2√2 × 2, and 2 × 2 unit cells along the surface planes and required 5 × 5 × 1, 4 × 5 × 1, and 5 × 5 × 1 *k*-point meshes, respectively. More details about the surface models are provided in Sec. IV.

### III. BULK TAC<sub>x</sub>N<sub>1-x</sub>

The calculated equilibrium lattice constant as a function of the bulk composition (or *x*) is shown in Fig. 2, along with

<sup>a)</sup>Electronic mail: rampi@ims.uconn.edu.

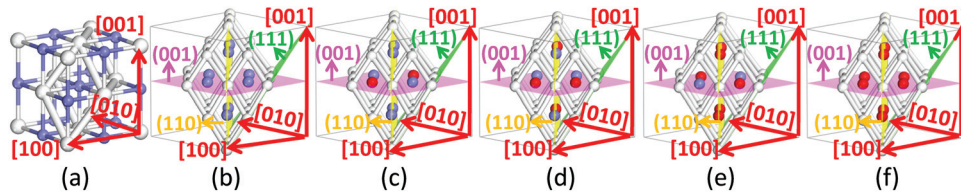


FIG. 1. (Color online) (a) The conventional cubic cell and primitive rhombohedral cell (the latter shown in white) of bulk TaN; (b) the  $2 \times 2 \times 2$  TaN supercell; and (c), (d), (e), and (f) the supercells of  $\text{TaC}_x\text{N}_{1-x}$  for  $x = 0.25, 0.5, 0.75,$  and  $1$ , respectively. Ta, C, and N atoms are represented by white, navy (gray), and red (dark gray) spheres, respectively. The, [001], [110], and [111] directions as well as the (001), (110) and (111) planes are indicated.

the experimental values of the end members ( $x=0$  or  $1$ ). Our computed lattice constants of pure TaN and TaC are 4.40 and 4.46 Å, respectively, identical to the corresponding experimental values.<sup>16</sup> Similar to  $\text{TiC}_x\text{N}_{1-x}$ ,<sup>10</sup> the equilibrium lattice parameter of  $\text{TaC}_x\text{N}_{1-x}$  increases with the carbon fraction ( $x$ ). By treating NaCl-type  $\text{TaC}_x\text{N}_{1-x}$  as a reaction product of TaC and TaN, we next define its formation energy,  $E_{\text{form}}$ , as follows:

$$E_{\text{form}} = E_{\text{TaC}_x\text{N}_{1-x}, \text{bulk}} - xE_{\text{TaC}, \text{bulk}} - (1-x)E_{\text{TaN}, \text{bulk}}, \quad (1)$$

where  $E_{\text{TaC}_x\text{N}_{1-x}, \text{bulk}}$ ,  $E_{\text{TaC}, \text{bulk}}$ , and  $E_{\text{TaN}, \text{bulk}}$  are the calculated DFT energies per Ta atom of the bulk  $\text{TaC}_x\text{N}_{1-x}$  alloy, pure TaC, and pure TaN, respectively. As also plotted in Fig. 2,  $E_{\text{form}}$  and hence the stability of NaCl-type  $\text{TaC}_x\text{N}_{1-x}$  increases with the carbon concentration ( $x$ ) in a similar way as the  $\text{TiC}_x\text{N}_{1-x}$  alloys. But the formation energy of  $\text{TaC}_x\text{N}_{1-x}$  is not all negative for the alloy compositions considered. As Fig. 2 shows,  $\text{TaC}_{0.25}\text{N}_{0.75}$  has a positive formation energy and hence tends to decompose. This finding is consistent with the prior report that NaCl-type  $\text{TaC}_x\text{N}_{1-x}$  will be stable when  $x > 0.4$ .<sup>11,17</sup> This phenomenon is probably due to the different equilibrium structures of TaN (CoSn type) and TaC (NaCl type).  $\text{TaC}_x\text{N}_{1-x}$  with a high N concentration is more likely to be stable in the CoSn-type rather than NaCl-type structure. Although NaCl-type  $\text{TaC}_{0.25}\text{N}_{0.75}$  is a metastable phase, it is still informative to investigate its surface stability and WF since the NaCl phase could be obtained by specific synthesis techniques.<sup>11</sup> Thus, all five compositions mentioned earlier were considered for the subsequent surface studies as described in Secs. IV and V.

To investigate the electronic structure change of a ternary  $\text{TaC}_x\text{N}_{1-x}$  system when substituting carbon atoms for nitrogen atoms, we have computed the total density of states

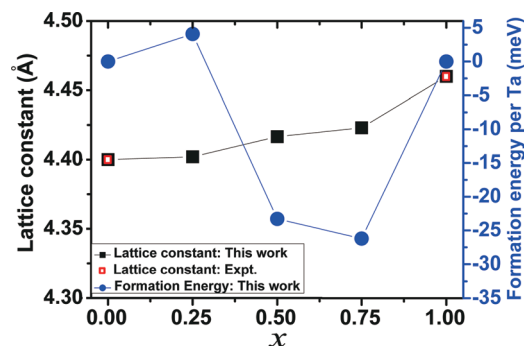


FIG. 2. (Color online) Lattice constants and formation energies per Ta of bulk  $\text{TaC}_x\text{N}_{1-x}$  as a function of  $x$ .

(DOS) of TaC,  $\text{TaC}_{0.5}\text{N}_{0.5}$ , and TaN in Fig. 3. The overall features are similar to those of previously published<sup>11,18</sup> carbides and nitrides. We can clearly see from Fig. 3 that these three compositions are all metallic and the DOS of  $\text{TaC}_{0.5}\text{N}_{0.5}$  is a combination of the DOS of TaC and TaN. Furthermore, the DOS at the Fermi level ( $E_F$ ) increases in the sequence:  $\text{TaC} \rightarrow \text{TaN} \rightarrow \text{TaC}_{0.5}\text{N}_{0.5}$ , consistent with the prior theoretical findings.<sup>11,18</sup> But we may note that in experiment TaC was always more electrically conductive than TaN, due to the fact that (1) the fabricated TaN is a mixture of a semiconductor phase (i.e.,  $\text{Ta}_3\text{N}_5$ ) and a metallic phase (i.e., NaCl-type TaN)<sup>5,12,19</sup> and (2) TaN is more likely to incorporate oxygen by postdeposition air exposure.<sup>20</sup>

#### IV. SURFACE ENERGY

We next focus on the energies of the (001), (110), and (111) surfaces of  $\text{TaC}_x\text{N}_{1-x}$ . These three specific orientations were considered as they are the normally observed ones.<sup>2,21</sup> As Fig. 1 shows, the composition and stacking sequence of the atomic planes are dependent on the bulk composition as well as the orientation. Table I summarizes all the possible stacking sequences along the three directions for a given bulk composition we considered. Symmetric slabs with identical top and bottom surfaces were applied in our work to study the properties of these possible surfaces. Among all the considered surfaces, only the (001) and (110) surfaces of TaN, TaC and  $\text{TaC}_{0.5}\text{N}_{0.5}$  are stoichiometric or nonpolar. All other surfaces are polar and hence require the specification of their surface energies in terms of the chemical potentials of the elemental components,<sup>10,22</sup> as will be described in detail in the following.

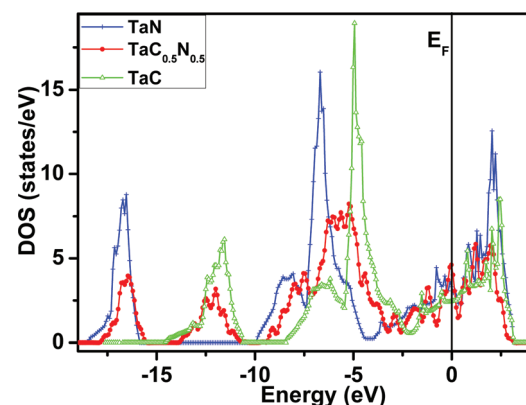


FIG. 3. (Color online) The total density of states for bulk TaC,  $\text{TaC}_{0.5}\text{N}_{0.5}$ , and TaN metal alloys. The Fermi levels ( $E_F$ ) of the three are matched up by shifting the DOS profiles.

TABLE I. The stacking sequences of  $\text{TaC}_x\text{N}_{1-x}$  along the  $\langle 001 \rangle$ ,  $\langle 110 \rangle$ , and  $\langle 111 \rangle$  directions.

Direction	Bulk composition				
	$x=0$	$x=0.25$	$x=0.5$	$x=0.75$	$x=1$
$\langle 001 \rangle$	TaN	TaC <sub>0.5</sub> N <sub>0.5</sub>	TaC <sub>0.5</sub> N <sub>0.5</sub>	TaC <sub>0.5</sub> N <sub>0.5</sub>	TaC
and	TaN	TaN	TaC <sub>0.5</sub> N <sub>0.5</sub>	TaC	TaC
$\langle 110 \rangle$	TaN	TaC <sub>0.5</sub> N <sub>0.5</sub>	TaC <sub>0.5</sub> N <sub>0.5</sub>	TaC <sub>0.5</sub> N <sub>0.5</sub>	TaC
	TaN	TaN	TaC <sub>0.5</sub> N <sub>0.5</sub>	TaC	TaC
	⋮	⋮	⋮	⋮	⋮
	⋮	⋮	⋮	⋮	⋮
$\langle 111 \rangle$	Ta	Ta	Ta	Ta	Ta
	N	CN <sub>3</sub>	CN	C <sub>3</sub> N	C
	Ta	Ta	Ta	Ta	Ta
	N	CN <sub>3</sub>	CN	C <sub>3</sub> N	C
	⋮	⋮	⋮	⋮	⋮

The surface energy ( $\sigma_{\text{surf}}$ ) can be computed based on DFT calculations, as the following indicates:

$$\sigma_{\text{surf}} = (E_{\text{slab}} - E_{\text{bulk}})/2A, \quad (2)$$

where  $E_{\text{slab}}$  and  $E_{\text{bulk}}$  are, respectively, the energies of the slab and of the bulk material with the same number and type of atoms as the slab.  $2A$  stands for the total area of the top and bottom surfaces.  $E_{\text{bulk}}$  could be expressed as

$$E_{\text{bulk}} = n_{\text{Ta}}\mu_{\text{Ta}} + n_{\text{C}}\mu_{\text{C}} + n_{\text{N}}\mu_{\text{N}}, \quad (3)$$

where  $\mu_{\text{Ta}}$ ,  $\mu_{\text{C}}$ , and  $\mu_{\text{N}}$  are the chemical potentials of Ta, C, and N atoms in bulk  $\text{TaC}_x\text{N}_{1-x}$ , respectively, and  $n_{\text{Ta}}$ ,  $n_{\text{C}}$ , and  $n_{\text{N}}$  are the number of Ta, C, and N atoms in the slab.

Since the DFT energy per Ta atom of the bulk  $\text{TaC}_x\text{N}_{1-x}$  alloy,  $E_{\text{TaC}_x\text{N}_{1-x}, \text{bulk}}$ , could be written as

$$E_{\text{TaC}_x\text{N}_{1-x}, \text{bulk}} = \mu_{\text{Ta}} + x\mu_{\text{C}} + (1-x)\mu_{\text{N}}, \quad (4)$$

the surface energy could be specified based on DFT energies and  $\mu_{\text{C}}$  and  $\mu_{\text{N}}$  as follows:

$$\sigma_{\text{surf}} = \{E_{\text{slab}} - n_{\text{Ta}}E_{\text{TaC}_x\text{N}_{1-x}, \text{bulk}} - (n_{\text{C}} - xn_{\text{Ta}})\mu_{\text{C}} - [n_{\text{N}} - (1-x)n_{\text{Ta}}]\mu_{\text{N}}\}/2A. \quad (5)$$

We note that for a stoichiometric or nonpolar surface [in which case  $n_{\text{Ta}}:n_{\text{C}}:n_{\text{N}} = 1:x:(1-x)$ ] the surface energy is uniquely specified and Eq. (5) could be simplified to

$$\sigma_{\text{surf}} = (E_{\text{slab}} - n_{\text{Ta}}E_{\text{TaC}_x\text{N}_{1-x}, \text{bulk}})/2A. \quad (6)$$

However, for polar surfaces, the surface energy is a function of  $\mu_{\text{C}}$  and  $\mu_{\text{N}}$  [cf. Eq. (5)]. By treating  $\mu_{\text{C}}$  and  $\mu_{\text{N}}$  as free parameters, we could determine the surface energy of the  $\langle 001 \rangle$ ,  $\langle 110 \rangle$ , and  $\langle 111 \rangle$  surfaces with various terminations and bulk compositions and find out the lowest energy surface for a given combination of  $\mu_{\text{C}}$  and  $\mu_{\text{N}}$ . This method has been used here to determine the surface stability for the five  $\text{TaC}_x\text{N}_{1-x}$  alloys, which is displayed in Fig. 4.

Moreover, we could further specify which surface is the most expected one for a given bulk composition by noting that the possible values  $\mu_{\text{C}}$  and  $\mu_{\text{N}}$  can take for a stable ternary alloy are limited by certain constraints.<sup>10,22</sup> To avoid elemental or binary compound segregation from the  $\text{TaC}_x\text{N}_{1-x}$  ternary,  $\mu_{\text{Ta}}$ ,  $\mu_{\text{C}}$ , and  $\mu_{\text{N}}$  should satisfy the following inequalities:

$$\begin{aligned} \mu_{\text{Ta}} &\leq \mu_{\text{Ta}, \text{bulk}} \\ \mu_{\text{C}} &\leq \mu_{\text{C}, \text{bulk}} \\ \mu_{\text{N}} &\leq \mu_{\text{N}_2, \text{gas}}/2 \\ \mu_{\text{Ta}} + \mu_{\text{C}} &\leq \mu_{\text{TaC}, \text{bulk}} \\ \mu_{\text{Ta}} + \mu_{\text{N}} &\leq \mu_{\text{TaN}, \text{bulk}} \\ 3\mu_{\text{C}} + 4\mu_{\text{N}} &\leq \mu_{\text{C}_3\text{N}_4, \text{bulk}}, \end{aligned} \quad (7)$$

where  $\mu_{\text{Ta}, \text{bulk}}$ ,  $\mu_{\text{C}, \text{bulk}}$ ,  $\mu_{\text{TaC}, \text{bulk}}$ ,  $\mu_{\text{TaN}, \text{bulk}}$ ,  $\mu_{\text{C}_3\text{N}_4, \text{bulk}}$ , and  $\mu_{\text{N}_2, \text{gas}}$  are the chemical potentials of bulk body-centered cubic Ta, graphite, NaCl-type TaC and TaN,  $\beta\text{-C}_3\text{N}_4$ , and gas phase  $\text{N}_2$ , respectively.

The above-mentioned inequalities could be further expressed as Eq. (8) with the following simplifications: (1) eliminating  $\mu_{\text{Ta}}$  from the above-mentioned inequalities according to Eq. (4); (2) replacing the bulk chemical potentials with the appropriate DFT energies by neglecting their temperature, or  $T$ , dependence; (3) representing  $\mu_{\text{N}_2, \text{gas}}$  as the sum of the DFT energy of  $\text{N}_2$ ,  $E_{\text{N}_2}$ , and its chemical potential change with temperature ( $T$ ) and  $\text{N}_2$  pressure ( $P_{\text{N}_2}$ ),  $\Delta\mu_{\text{N}_2, \text{gas}}(T, P_{\text{N}_2})$ ,

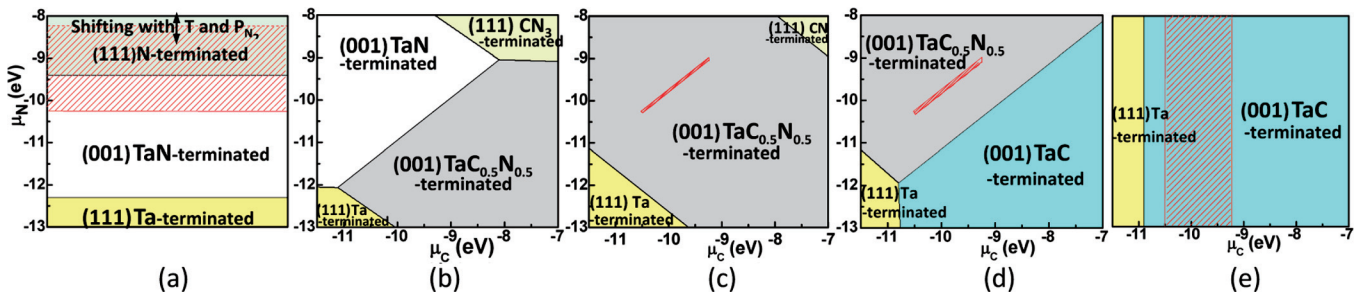


FIG. 4. (Color online) Surface stability of  $\text{TaC}_x\text{N}_{1-x}$  alloy for (a)  $x=0$ , (b)  $x=0.25$ , (c)  $x=0.5$ , (d)  $x=0.75$ , and (e)  $x=1.0$ . The lowest energy surface for each  $(\mu_{\text{C}}, \mu_{\text{N}})$  combination is indicated. The hatched area represents the allowed ranges of  $\mu_{\text{C}}$  and  $\mu_{\text{N}}$  within which  $\text{TaC}_x\text{N}_{1-x}$  is stable to decomposition. In (a) and (e), surface energies depend only on  $\mu_{\text{N}}$  and  $\mu_{\text{C}}$ , respectively. The upper boundary in (a) can shift based on the  $T$  and  $P_{\text{N}_2}$ .



$$\begin{aligned}
\mu_C &\leq E_{C,\text{bulk}} \\
\mu_N &\leq [E_{N_2} + \Delta\mu_{N_2,\text{gas}}(T, P_{N_2})]/2 \\
3\mu_C + 4\mu_N &\leq E_{C_3N_4,\text{bulk}} \\
x\mu_C + (1-x)\mu_N &\geq E_{\text{TaC}_x\text{N}_{1-x},\text{bulk}} - E_{\text{Ta},\text{bulk}} \\
\mu_C - \mu_N &\leq (E_{\text{TaC}_x\text{N}_{1-x},\text{bulk}} - E_{\text{TaC},\text{bulk}})/(x-1) \\
\mu_C - \mu_N &\geq (E_{\text{TaC}_x\text{N}_{1-x},\text{bulk}} - E_{\text{TaN},\text{bulk}})/x.
\end{aligned} \tag{8}$$

The inequalities in Eq. (8) bound  $\mu_C$  and  $\mu_N$  within the hatched areas in Fig. 4 [with the exception of Fig. 4(b), as discussed further in the following]. These are the “allowed” ( $\mu_C$  and  $\mu_N$ ) combination for  $\text{TaC}_x\text{N}_{1-x}$  to be stable to decomposition. The surface stability for the five bulk compositions [shown in Figs. 4(a)–4(e)] will be discussed in sequence.

As Fig. 4(a) represents, the upper boundary of the allowed range for TaN shifts with temperature ( $T$ ) and  $\text{N}_2$  pressure ( $P_{\text{N}_2}$ ) in the same manner as TiN.<sup>10</sup> For example, it may move upwards with the increase of  $P_{\text{N}_2}$  or the decrease of  $T$ . Thus depending on the  $\text{N}_2$  gas condition, the allowed range of TaN could purely lie in (001) TaN-terminated region or also cover (111) N-terminated region. In other words, the dominant orientation for the stable TaN may change between (001) and (111), which is in agreement with prior work by Nie *et al.*<sup>23</sup> By using reactive radio-frequency magnetron sputtering, they successfully grew NaCl-type TaN films on silicon substrates in various  $\text{N}_2/\text{Ar}$  ratios (the total processing ambient gas pressure was kept at 5.0 mTorr). They found that when  $\text{N}_2$  partial pressure increases from 15% to 30%, the dominant orientation changes from (001) to (111).

Figure 4(b) indicates that  $\text{TaC}_{0.25}\text{N}_{0.75}$  is not stable to decomposition (as already anticipated based on the results of Fig. 2). This finding is different from what we found for  $\text{TiC}_{0.25}\text{N}_{0.75}$  [stable over a certain chemical potential range that favors (001) TiN-terminated surface]. Moreover, the allowed chemical potential of  $\text{TaC}_{0.5}\text{N}_{0.5}$ , similar to  $\text{TiC}_{0.5}\text{N}_{0.5}$ , falls entirely in (001)  $\text{TaC}_{0.5}\text{N}_{0.5}$ -terminated surface [cf. Fig. 4(c)]. Figure 4(d) shows that  $\text{TaC}_{0.75}\text{N}_{0.25}$  metal alloy has a larger allowed range than  $\text{TaC}_{0.5}\text{N}_{0.5}$  and thus is more stable. Similar to  $\text{TiC}_{0.75}\text{N}_{0.25}$ , the stable surface for  $\text{TaC}_{0.75}\text{N}_{0.25}$  metal alloy is (001)  $\text{TaC}_{0.5}\text{N}_{0.5}$ -terminated surface. Finally, we can tell from Fig. 4(e) that the allowed

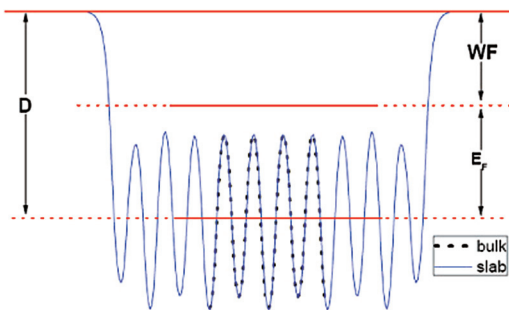


FIG. 5. (Color online) Schematic of the planar averaged potential,  $V_{\text{avg},z}$ , for the bulk (dashed line) and surface (solid line).  $E_F$  is the Fermi energy of the bulk. The planar averaged potential for the surface is shifted so that it matches with the bulk potential. The energy difference between the vacuum level ( $D$ ) and the bulk Fermi energy ( $E_F$ ) is the WF.

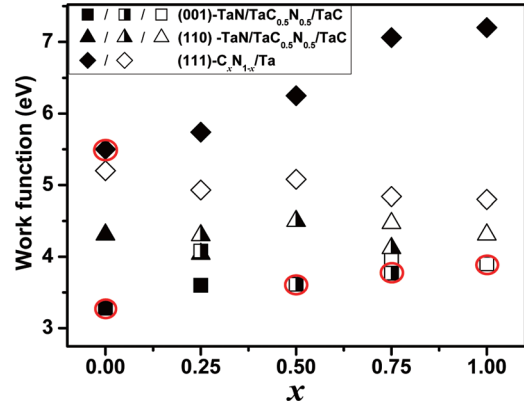


FIG. 6. (Color online) Work function for all  $\text{TaC}_x\text{N}_{1-x}$  surface orientations and terminations considered. The circled data correspond to the WF of the stable surfaces.

range of TaC binary entirely falls in (001) TaC-terminated surface. However, our prior knowledge for TiC indicates that (001) TiC-terminated and (111) Ti-terminated surfaces could both be stable in the allowed range of TiC binary. In sum, the surface stability diagrams for  $\text{TaC}_x\text{N}_{1-x}$  and  $\text{TiC}_x\text{N}_{1-x}$  are very similar, although there exist several interesting discrepancies as discussed earlier.

## V. WORK FUNCTION

Finally, we calculated the vacuum WF for each of the above-considered surfaces. As WF is the energy required to extract one electron out of the metal surface into the vacuum region, it can be written as  $D - E_F$ , where  $D$  is the electrostatic potential in the vacuum region and  $E_F$  is the Fermi energy of the metal (cf. Fig. 5). To avoid quantum size effects,<sup>24</sup> we applied the following procedure to determine the WF.<sup>25,26</sup> The planar averaged local electronic potential ( $V_{\text{avg},z}$ ) normal to the surface and that of the corresponding bulk along the same direction are calculated individually. We found that two layers away from the surface the potential already recovers the form of the bulk potential, although shifted by a constant amount. By matching the two planar averaged potentials and knowing the bulk Fermi energy relative to the bulk  $V_{\text{avg},z}$ , as schematically shown in Fig. 5, we calculate the WF as the difference between the vacuum energy ( $D$ ) and the bulk Fermi energy ( $E_F$ ).

The computed WFs for all surfaces we considered are collected and portrayed in Fig. 6. We note that the surface

TABLE II. Work functions for (001) surfaces of TaC, TaN, TiC, and TiN.

	TaC	TaN	TiC	TiN
Our work	3.80	3.30	4.55	3.20
Prior DFT	3.61 <sup>a</sup>	3.45 <sup>b</sup>	4.62 <sup>b</sup>	3.25 <sup>b</sup>
Experiment	4.3 <sup>c</sup>	4.0 <sup>d</sup>	3.8 <sup>e</sup>	2.92 <sup>d</sup>

<sup>a</sup>Reference 8.

<sup>b</sup>Reference 9.

<sup>c</sup>Reference 27.

<sup>d</sup>Reference 30.

<sup>e</sup>Reference 29.

TABLE III. Work functions for (001) defective surfaces of TaC, TaN, and TiC.

	TaC	TaN	TiC
Our work			
(1) No surface vacancies	3.80	3.30	4.55
(2) 50% surface C or N vacancies	4.17	3.33	4.06
(3) 100% surface C or N vacancies	4.29	4.52	3.51
(4) 50% surface Ta or Ti vacancies	5.18	4.31	5.64
(5) 100% surface Ta or Ti vacancies	7.25	9.0	7.11

termination has a larger influence on the WF than the bulk composition, which is similar to what we found for  $\text{TiC}_x\text{N}_{1-x}$ . Among all the surfaces, the (111) surfaces, especially  $\text{C}_x\text{N}_{1-x}$ -terminated (111) surfaces, have a relatively high WF. Based on the surface stability studies in Sec. IV, we further circled the WFs for the stable surfaces of  $\text{TaC}_x\text{N}_{1-x}$ . The WF for the (001) stable surfaces increases monotonically from the pure TaN value of 3.3 eV to the pure TaC value of 3.8 eV. As discussed before, depending on the temperature and  $\text{N}_2$  pressure, the dominant orientation of TaN may change between (001) TaN-terminated and (111) N-terminated surfaces with a WF of 3.3 and 5.5 eV, respectively. Thus, the WF of TaN could be tuned to a large degree by varying T and  $P_{\text{N}_2}$ .

Table II lists the calculated WFs for the (001) surface of TaC, TaN, TiC, and TiN. The predicted WF is in agreement with prior DFT predictions in general. The important feature of Table II is that all the DFT WFs are slightly off with respect to the corresponding experimental values.<sup>27–30</sup> For example, DFT determinations are smaller than the experimental values for (001) TaC and TaN, but larger than the experimental result for (001) TiC. In fact, such discrepancies have been reported and explored before for the (001) TiC surface by Price *et al.*<sup>7</sup> and Zhu *et al.*<sup>10</sup> Both works indicate that the carbon vacancies in experimental TiC samples were most likely to be responsible for the difference between theory and experiment.<sup>7</sup> In order to explore this further, we calculated the WF for (001) defective surfaces of TaC (TaN) with 100% and 50% Ta or C (N) vacancies in the surface plane, as listed in Table III (which also contains our prior results for TiC). One of the interesting findings is that the surface vacancies have a significant impact on the WF, especially for the Ta or Ti vacancies. Furthermore, we note that any surface vacancy (Ta, C, or N vacancy) is able to increase the WF of TaC and TaN, which is different from TiC (carbon vacancies reduce the WF). When 50% C vacancies were introduced to a perfect (001) surface of TaC, the WF would increase by 0.37 eV (cf. Table III), in agreement with the prior experimental studies by Gruzalski *et al.*<sup>28</sup> On the other hand, the WF for the (001) surface of TiC would decrease by 0.49 eV when the surface carbon vacancy concentration increases from 0% to 50%.<sup>10</sup> This finding explains why the experimental determinations for TaC and TaN (TiC) are larger (smaller) than DFT results.

## VI. CONCLUSION

We have applied DFT calculations to study the bulk and surface properties of ordered  $\text{TaC}_x\text{N}_{1-x}$  alloys for several

carbon concentrations ( $x$ ). The results of this work could be summarized as follows:

- The stability of NaCl-type  $\text{TaC}_x\text{N}_{1-x}$  ternary to decomposition to TaC and TaN will increase with the carbon concentration ( $x$ ).
- Through computing the chemical potential dependent surface energy and determining the allowed ( $\mu_{\text{C}}$ ,  $\mu_{\text{N}}$ ) combination for stable alloys, we have determined the most probable terminations for  $\text{TaC}_x\text{N}_{1-x}$ , except for  $\text{TaC}_{0.25}\text{N}_{0.75}$  (for which no allowed range of chemical potentials exist). Depending on the  $\text{N}_2$  condition, the stable termination for TaN could be (001) TaN-terminated non-polar surface or (111) N-terminated polar surface. For  $\text{TaC}_{0.5}\text{TaC}_{0.5}$ ,  $\text{TaC}_{0.75}\text{N}_{0.25}$ , and TaC alloys, the favored termination is (001)  $\text{TaC}_{0.5}\text{N}_{0.5}$ ,  $\text{TaC}_{0.75}\text{N}_{0.25}$ , and TaC terminated, respectively.
- WF studies on  $\text{TaC}_x\text{N}_{1-x}$  reveal that the WF of these (001) stable surfaces increases monotonically from the pure TaN value of 3.3 eV to the pure TaC value of 3.8 eV. However, this variation is far surpassed by its dependence on the surface orientation and defect density (regardless of the alloy composition).
- The discrepancy between WF obtained from DFT calculations and that from experiment for TaC, TaN, and TiC is analyzed. The vacancies in experimental samples were most likely responsible for this discrepancy.
- Work function “tuning” may be accomplished by suitably controlling the surface chemistry for any stable  $\text{TaC}_x\text{N}_{1-x}$  alloy composition.

## ACKNOWLEDGMENTS

Financial support of this work through a grant from the National Science Foundation (NSF) and computational support through a NSF Teragrid Resource Allocation are gratefully acknowledged. R.R. would also like to acknowledge a fellowship from the Alexander von Humboldt Foundation.

- <sup>1</sup>M. Wittmer, *J. Vac. Sci. Technol. A* **3**, 1797 (1985).
- <sup>2</sup>H. O. Pierson, *Handbook of Refractory Carbides and Nitrides: Properties, Characteristics and Applications* (Noyes, Westwood, NJ, 1996).
- <sup>3</sup>J. Robertson, *Rep. Prog. Phys.* **69**, 327 (2006); R. M. Wallace and G. D. Wilk, *Crit. Rev. Solid State Mater. Sci.* **28**, 231 (2003).
- <sup>4</sup>S.-H. Joo, C.-R. Paik, and K.-H. Lee, U.S. patent 5,795,817 (18 August 1998).
- <sup>5</sup>J. K. Schaeffer, C. Capasso, R. Gregory, D. Gilmer, L. R. C. Fonseca, M. Raymond, C. Happ, M. Kottke, S. B. Samavedam, P. J. Tobin, and B. E. White, *J. Appl. Phys.* **101**, 014503 (2007).
- <sup>6</sup>S. H. Jhi, J. Ihm, S. G. Louie, and M. L. Cohen, *Nature (London)* **399**, 132 (1999); H. W. Hugosson, O. Eriksson, U. Jansson, and B. Johansson, *Phys. Rev. B* **63**, 134108 (2001); B. Kolb and G. L. W. Hart, *ibid.* **72**, 224207 (2005).
- <sup>7</sup>D. L. Price, J. M. Wills, and B. R. Cooper, *Phys. Rev. B* **48**, 15311 (1993).
- <sup>8</sup>F. Vines, C. Sousa, and F. Illas, *J. Phys. Chem. C* **111**, 1307 (2007).
- <sup>9</sup>K. Kobayashi, *Surf. Sci.* **493**, 665 (2001).
- <sup>10</sup>H. Zhu, M. Aindow, and R. Ramprasad, *Phys. Rev. B* **80**, 201406(R) (2009).
- <sup>11</sup>A. A. Lavrentyev, B. V. Gabrelian, V. B. Vorzhev, I. Ya. Nikiforov, and O. Yu. Khyzhun, *J. Alloys Compd.* **472**, 104 (2009).
- <sup>12</sup>J.-D. Kwon, J. Yun, and S.-W. Kang, *Jpn. J. Appl. Phys.* **48**, 025504 (2009).
- <sup>13</sup>G. Kresse and J. Furthmuller, *Phys. Rev. B* **54**, 11169 (1996).
- <sup>14</sup>J. P. Perdew, J. A. Chevary, S. H. Vosko, K. A. Jackson, M. R. Pederson, D. J. Singh, and C. Fiolhais, *Phys. Rev. B* **46**, 6671 (1992).

- <sup>15</sup>D. Vanderbilt, *Phys. Rev. B* **41**, R7892 (1990).
- <sup>16</sup>P. M. McKenna, *Ind. Eng. Chem.* **28**, 767 (1936); H. B. Nie, S. Y. Xu, and S. J. Wang, *Appl. Phys. A* **73**, 229 (2001).
- <sup>17</sup>H. J. Goldschmidt, *Interstitial Alloys* (Butterworths, London, 1967).
- <sup>18</sup>M. Sahnoun, C. Daul, M. Dri, J. C. Parlebas, and C. Demangeat, *Comput. Mater. Sci.* **33**, 175 (2005).
- <sup>19</sup>C. Stampfl and A. J. Freeman, *Phys. Rev. B* **71**, 024111 (2005).
- <sup>20</sup>M.-K. Song and S.-W. Rhee, *Chem. Vap. Deposition* **14**, 334 (2008).
- <sup>21</sup>A. Azushima, Y. Tanno, H. Iwata, and K. Aoki, *Wear* **265**, 1017 (2008).
- <sup>22</sup>K. Reuter and M. Scheffler, *Phys. Rev. B* **65**, 035406 (2001); S. J. Jenkins, *ibid.* **70**, 245401 (2004).
- <sup>23</sup>H. B. Nie, S. Y. Xu, S. J. Wang, L. P. You, Z. Yang, C. K. Ong, J. Li, and T. Y. F. Liew, *Appl. Phys. A* **73**, 229 (2001).
- <sup>24</sup>C. J. Fall, N. Binggeli, and A. Baldereschi, *J. Phys. Condens. Matter* **11**, 2689 (1999).
- <sup>25</sup>C. G. Van de Walle and R. M. Martin, *Phys. Rev. B* **34**, 5621 (1986).
- <sup>26</sup>R. Ramprasad, P. von Allmen, and L. R. C. Fonseca, *Phys. Rev. B* **60**, 6023 (1999).
- <sup>27</sup>T. Aizawa, Report of the National Institute for Research in Inorganic Materials 81 (1994).
- <sup>28</sup>G. R. Gruzalski, S.-C. Lui, and D. M. Zehner, *Surf. Sci. Lett.* **239**, L517 (1990).
- <sup>29</sup>C. Oshima, T. Tanaka, M. Aono, R. Nishitani, S. Zaima, and F. Yajima, *Appl. Phys. Lett.* **35**, 822 (1979).
- <sup>30</sup>Y. Saito, S. Kawata, H. Nakane, and H. Adachi, *Appl. Surf. Sci.* **146**, 177 (1999).